Physics Letters B 800 (2020) 135133

Contents lists available at ScienceDirect

Physics Letters B

www.elsevier.com/locate/physletb

# Constraining nuclear physics parameters with current and future COHERENT data

D.K. Papoulias [a,*], T.S. Kosmas [b], R. Sahu [c], V.K.B. Kota [d], M. Hota [c]

[a] AHEP Group, Instituto de Física Corpuscular – C.S.I.C./Universitat de València, Edificio de Institutos de Paterna, C/Catedratico José Beltrán, 2 E-46980 Paterna (València), Spain
[b] Division of Theoretical Physics, University of Ioannina, GR 45110 Ioannina, Greece
[c] National Institute of Science and Technology, Palur Hills, Berhampur - 761008, Odisha, India
[d] Physical Research Laboratory, Ahmedabad 380 009, India

ARTICLE INFO

*Article history:*
Received 19 March 2019
Received in revised form 6 September 2019
Accepted 27 November 2019
Available online 2 December 2019
Editor: J.-P. Blaizot

*Keywords:*
Coherent neutrino elastic neutrino-nucleus scattering
COHERENT experiment
Deformed shell model
Weak neutron form factors

ABSTRACT

Motivated by the recent observation of coherent elastic neutrino-nucleus scattering (CE$\nu$NS) at the COHERENT experiment, our goal is to explore its potential in probing important nuclear structure parameters. We show that the recent COHERENT data offers unique opportunities to investigate the neutron nuclear form factor. Our present calculations are based on the deformed Shell Model (DSM) method which leads to a better fit of the recent CE$\nu$NS data, as compared to known phenomenological form factors such as the Helm-type, symmetrized Fermi and Klein-Nystrand. The attainable sensitivities and the prospects of improvement during the next phase of the COHERENT experiment are also considered and analyzed in the framework of two upgrade scenarios.



## 1. Introduction

The recent observation of coherent elastic neutrino nucleus scattering (CE$\nu$NS) events at the Spallation Neutron Source (SNS) by the COHERENT experiment [1,2], has opened up new opportunities to probe physics in theories within and beyond the Standard Model (SM) of electroweak interactions. The COHERENT program is aiming to investigate several important physical phenomena through low-energy precision measurements. The first CE$\nu$NS observation has triggered the theoretical challenges required to interpret neutrino-nuclear responses [3] in the context of new physics models [4].

Recently, several studies were conducted in trying to analyze and interpret the COHERENT data, in order to examine possible deviations from the SM predictions that may point to new physics [5,6]. These searches address non-standard interactions (NSIs) [7–10], electromagnetic (EM) properties [11–13], sterile neutrinos [14–16], novel mediators [17–20], CP-violation [21,22] and implications to dark matter [23–25]. Potential contributions due to neutrino-nucleus scattering at direct dark matter detection detectors have been explored [26–29], while the CE$\nu$NS cross section has been also revisited within [30] and beyond the SM [31–33].

The nuclear form factor related to weak interactions plays a dominant role in the accurate description of neutrino-matter interactions [75] motivating further the necessity of revisiting the relevant nuclear parameters (see Refs. [34,76]). While neutrinos are a valuable tool for deep sky investigations [77], nuclear parameters such as the neutron skin can be crucial for understanding neutron star dynamics [78]. In this work we explore how such nuclear parameters can be probed at CE$\nu$NS experiments. For realistic nuclear structure calculations, we employ the deformed shell model (DSM) based on Hartree-Fock (HF) deformed intrinsic states with angular momentum projection and band mixing [35]. The DSM has been previously applied for describing nuclear spectroscopic properties [35–37], exotic processes such as $\mu \to e$ conversion in nuclei [38] and WIMP-nucleus scattering [39].

The conventional neutrino-processes are theoretically well-studied [40,41], while the recent CE$\nu$NS observation motivates precision tests of the SM at low energies [42]. It has been shown that a competitive determination of the weak-mixing angle is possible [43], while CE$\nu$NS also highlights a novel avenue for probing the neutron nuclear form factor [34,44,45]. During its phase I, the

* Corresponding author.
*E-mail addresses:* dipapou@ific.uv.es (D.K. Papoulias), hkosmas@uoi.gr (T.S. Kosmas), rankasahu@gmail.com (R. Sahu), vkbkota@prl.res.in (V.K.B. Kota), mihirhota@nist.edu (M. Hota).

https://doi.org/10.1016/j.physletb.2019.135133

COHERENT collaboration achieved a high experimental sensitivity and a low detector threshold which led to the first observation of CE$\nu$NS while also intends to enhance its future program with a multitarget strategy [46]. Apart from the next phase of COHERENT, other experiments are planned to operate with reactor neutrinos like the TEXONO [47], CONNIE [48], MINER [49], $\nu$GEN [50], CONUS [51], Ricochet [52] and NU-CLEUS [53], further motivating the present work.

Muon spectroscopy [54] and atomic parity violating (APV) electron scattering data [55] from the PREX experiment [56] has been employed as a powerful tool to measure the spatial distributions of neutrons in nuclei [57–59]. Our paper focuses on the open issues related to constraining the nuclear physics parameters [60,61] entering the description of the weak neutral current vector and axial vector properties, such as ground state properties mostly related to the dominance of neutrons participating in the materials of rare-events detectors [62]. On the basis of our nuclear DSM calculations and the COHERENT data, we will make an attempt to extract constraints on the nuclear form factors in the Helm [63], symmetrized Fermi [64] and Klein-Nystrand [65] approach, as well as to explore the neutron radial moments [66].

The paper has been organized as follows: in Sect. 2 we present the relevant formalism to accurately simulate the COHERENT data, while in Sect. 3 we introduce the DSM method and discuss the various form factor parametrizations considered. Sect. 4 presents the main outcomes of this work and finally in Sect. 5 the main conclusions are discussed.

## 2. CE$\nu$NS within deformed shell model calculations

Within the framework of the SM, the CE$\nu$NS differential cross section with respect to the nuclear recoil energy $T_A$ is written as [4,27]

$$\frac{d\sigma}{dT_A} = \frac{G_F^2 m_A}{\pi}\left[G_V^2\left(1-\frac{m_A T_A}{2E_\nu^2}\right)+G_A^2\left(1+\frac{m_A T_A}{2E_\nu^2}\right)\right], \tag{1}$$

where $G_F$ is the Fermi coupling constant, $E_\nu$ is the neutrino energy and $m_A$ the nuclear mass of the target $(A, Z)$, with $Z$ protons and $N = A - Z$ neutrons ($A$ is the mass number). The vector and axial vector weak charges $G_V$ and $G_A$, depend on the momentum variation of the proton and neutron nuclear form factors $F_p(Q^2)$ and $F_n(Q^2)$, as [30]

$$\begin{aligned} G_V(Q) &= \left[g_p^V Z F_p(Q^2) + g_n^V N F_n(Q^2)\right], \\ G_A(Q) &= \left[g_p^A(\delta Z) F_p(Q^2) + g_n^A(\delta N) F_p(Q^2)\right], \end{aligned} \tag{2}$$

with the vector couplings for protons and neutrons taken as $g_p^V = 1/2 - 2\sin^2\theta_W$ and $g_n^V = -1/2$ respectively, and the weak mixing angle $\theta_W$ fixed to the PDG value $\sin^2\theta_W = 0.2312$ [68]. The corresponding axial vector couplings for protons and neutrons are defined as $g_p^A = 1/2$ and $g_n^A = -1/2$, while $(\delta Z) = Z_+ - Z_-$ and $(\delta N) = N_+ - N_-$, where the $+$ or $-$ sign accounts for the total number of protons or neutrons with spin up and down, respectively [5]. Note that the $g_A$ couplings are quenched for charged-current processes (see Refs. [3,69]).

The COHERENT experiment has made the first ever observation of CE$\nu$NS with a CsI[Na] detector of mass $m_{\rm det} = 14.57$ kg exposed to neutrino emissions from the $\pi$-DAR source at a distance of $L = 19.3$ m, for a period of $t_{\rm run} = 308.1$ days. To adequately simulate the recent COHERENT data we consider the total cross section as the sum of the individual cross sections by taking also into account the stoichiometric ratio $\eta$ of the corresponding atom. For a given neutrino flavor $\alpha$ and isotope $x$, the number of CE$\nu$NS events reads [4]

$$\begin{aligned} N_{\rm theor} = \sum_{\nu_\alpha}\sum_{x={\rm Cs,I}} \mathcal{F}_x \int_{E_\nu^{\rm min}}^{E_\nu^{\rm max}} \lambda_{\nu_\alpha}(E_\nu) dE_\nu \\ \times \int_{T_A^{\rm min}}^{T_A^{\rm max}} \mathcal{A}(T_A)\frac{d\sigma_x}{dT_A}(E_\nu, T_A) dT_A\,, \end{aligned} \tag{3}$$

where

$$\mathcal{F}_x = t_{\rm run} N_{\rm targ}^x \Phi_\nu\,. \tag{4}$$

The neutrino flux is $\Phi_\nu = r\mathcal{N}_{\rm POT}/4\pi L^2$, with $r = 0.08$ representing the number of neutrinos per flavor produced for each proton on target (POT), where $\mathcal{N}_{\rm POT} = N_{\rm POT}/t_{\rm run}$ with $N_{\rm POT} = 1.76\times 10^{23}$. Our calculations consider the Geant4 SNS neutrino spectrum taken from the upper panel of Fig. S2 shown in Ref. [1]. Here, the various flavor components $\nu_\alpha = \{\nu_e, \nu_\mu, \bar{\nu}_\mu\}$ of the SNS neutrino spectrum, including also the monochromatic $E_{\nu_\mu} = 29.9$ MeV prompt beam from pion decay at rest, are denoted as $\lambda_{\nu_\alpha}(E_\nu)$, while for each isotope $x = {\rm Cs, I}$, the number of target nuclei is expressed in terms of Avogadro's number $N_A$ and the detector mass

$$N_{\rm targ}^x = \frac{m_{\rm det}\eta_x}{\sum_x A_x \eta_x} N_A\,. \tag{5}$$

We furthermore stress that contributions to event rate from the sodium dopant are of the order $10^{-5}$–$10^{-4}$ and can be safely ignored [70].

The recent observation of the CE$\nu$NS signal at COHERENT experiment was based on photoelectron (PE) measurements. To translate the nuclear recoil energy in terms of the number of PE, $n_{\rm PE}$, we adopt the relation [1]

$$n_{\rm PE} = 1.17\frac{T_A}{({\rm keV})}\,. \tag{6}$$

In Eq. (3), the photoelectron dependence of the detector efficiency $\mathcal{A}(x)$ is given by the expression [2]

$$\mathcal{A}(x) = \frac{k_1}{1+e^{-k_2(x-x_0)}}\Theta(x)\,, \tag{7}$$

with parameters $k_1 = 0.6655$, $k_2 = 0.4942$, $x_0 = 10.8507$ and $\Theta(x)$ being the Heaviside function, defined as

$$\Theta(x) = \begin{cases} 0 & x < 5 \\ 0.5 & 5 \le x < 6 \\ 1 & x \ge 6\,. \end{cases} \tag{8}$$

## 3. Evaluation of the nuclear form factors

In CE$\nu$NS and direct dark matter detection searches, to account for the finite nuclear size, the nuclear form factor is defined as the Fourier transform of the nuclear charge density distribution [40]

$$F_{n,p}(Q^2) = \frac{1}{N_a}\int \rho_{p,n}(\vec{r})\, e^{i\vec{Q}\cdot\vec{r}}\, d^3\vec{r}, \quad N_a = Z, N\,, \tag{9}$$

with $F_p \neq F_n$. Following a model independent approach, the nuclear form factor can be expanded in terms of even moments of the charge density distribution [44]

$$F_{p,n}(Q^2) \approx 1 - \frac{Q^2}{3!}\langle R_{p,n}^2\rangle + \frac{Q^4}{5!}\langle R_{p,n}^4\rangle - \frac{Q^6}{7!}\langle R_{p,n}^6\rangle + \cdots\,, \tag{10}$$

**Table 1**
The calculated magnetic moments and their decomposition into orbital and spin parts for the ground states of $^{127}$I and $^{133}$Cs. The magnetic moments given in column 9 are obtained by multiplying the entries in columns 5-8 with the bare gyromagnetic ratios (in nm units) $g_l^p = 1$, $g_l^n = 0$, $g_s^p = 5.586$ and $g_s^n = -3.826$ and then summing. Shown in the table are also the ground state $J^\pi$ and the harmonic oscillator size parameter $b$ employed in the calculations. The experimental data are taken from Ref. [67].

| Nucleus | $A$ | $Z$ | $J^\pi$ | $< l_p >$ | $< S_p >$ | $< l_n >$ | $< S_n >$ | $\mu$ (nm) | Exp (nm) | $b$ [fm$^{-1}$] |
|---|---|---|---|---|---|---|---|---|---|---|
| I | 127 | 53 | $5/2^+$ | 2.395 | −0.211 | 0.313 | 0.002 | 1.207 | 2.813 | 2.09 |
| Cs | 133 | 55 | $7/2^+$ | 3.40 | −0.339 | 0.49 | −0.048 | 1.69 | 2.582 | 2.11 |

with the $k$-th radial moment defined as

$$\langle R^k_{p,n} \rangle = \frac{\int \rho_{p,n}(\vec{r})\, r^k\, d^3\vec{r}}{\int \rho_{p,n}(\vec{r})\, d^3\vec{r}}\,. \tag{11}$$

From experimental physics perspectives, it is feasible to measure only the proton charge density distribution with high precision from electron scattering data [55]. For this reason, numerous studies rely on the approximation $\rho_p = \rho_n$ and thus assume $F_p = F_n$. On the theoretical side, both the proton and neutron nuclear form factors can be treated separately, within the context of advanced nuclear physics methods such as, the large-scale Shell-Model [71,72], the Quasiparticle Random Phase Approximation (QRPA) [73], Microscopic Quasiparticle Phonon Model (MQPM) [41] and the method of DSM calculations [27]. In the present work we employ the latter method. Our primary goal is to extract crucial information on the nuclear parameters entering the various form factor approaches from the recent data of the COHERENT experiment, relying on the various definitions of the nuclear form factor that we consider in the present study.

In the concept of DSM, for the calculation of the form factors relevant to the COHERENT detector materials $^{127}$I and $^{133}$Cs, we have adopted an effective interaction recently developed in Ref. [74] employing a model space consisting of the spherical orbitals $0g_{7/2}$, $1d_{5/2}$, $1d_{3/2}$, $2s_{1/2}$ and $0h_{11/2}$ with the closed core $^{100}$Sn. The effective interaction is obtained by renormalizing the CD-Bonn potential. The single particle energies for the five orbitals are taken to be 0.0, 0.4, 1.4, 1.3 and 1.6 MeV for protons and 0.0, 0.7, 2.1, 1.9 and 3.0 MeV for neutrons. We first perform an axially symmetric HF calculation and obtain the lowest intrinsic solution using the above effective interaction for each of the above nuclei. Then, excited intrinsic states are obtained by making particle-hole excitations over the lowest intrinsic states. At the final step, we perform angular momentum projection and band mixing and obtain the nuclear wave functions which are used for calculating different properties of these nuclei. We stress that including more orbits requires a new effective interaction that is beyond the scope of the present paper.

We have considered six intrinsic configurations for $^{127}$I and three intrinsic configurations for $^{133}$Cs. These intrinsic states are found to be sufficient to produce most of the important properties of these isotopes (complete details will be reported elsewhere). In Table 1, we tabulate the most important observables and outcomes of the nuclear structure calculations from DSM in the present work. Specifically, the observables include the magnetic moments of the two nuclei considered and the contribution of protons and neutrons to the orbital and spin parts giving better physical insight. Magnetic moments and spectroscopic properties of the two nuclei are calculated to check the reliability of the nuclear wave functions generated by DSM.

Besides realistic nuclear structure calculations within DSM, a rather reliable description of the nuclear form factor is the known as Helm approximation. The latter relies on the convolution of two nucleonic densities, one being a uniform density with cut-off radius, $R_0$, (namely box or diffraction radius) characterizing the interior density and a second one that is associated with a Gaussian falloff in terms of the surface thickness, $s$. In the Helm approximation the form factor is expressed in analytical form as [63]

$$F_{\rm Helm}(Q^2) = 3\frac{j_1(Q R_0)}{q R_0}\, e^{-(Q s)^2/2}\,, \tag{12}$$

where $j_1(x)$ denotes the 1st-order spherical Bessel function. The first three moments can be analytically expressed as [66]

$$\begin{aligned}
\left\langle R_n^2 \right\rangle &= \frac{3}{5}R_0^2 + 3s^2 \\
\left\langle R_n^4 \right\rangle &= \frac{3}{7}R_0^4 + 6R_0^2 s^2 + 15 s^4 \\
\left\langle R_n^6 \right\rangle &= \frac{1}{3}R_0^6 + 9R_0^4 s^2 + 63 R_0^2 s^4 + 105 s^6\,.
\end{aligned} \tag{13}$$

Following Ref. [62] we fix an *ad-hoc* value $s = 0.9$, obtained by fitting to muon spectroscopy data [54]. The latter has the advantage of improving the matching between the Helm and the symmetrized Fermi (SF) form factor that is discussed below. Adopting a conventional Fermi (Woods-Saxon) charge density distribution, the SF form factor is written in terms of two parameters $(c, a)$ in analytical form, as [64]

$$\begin{aligned}
F_{\rm SF}\left(Q^2\right) = &\frac{3}{Q c\left[(Q c)^2 + (\pi Q a)^2\right]}\left[\frac{\pi Q a}{\sinh(\pi Q a)}\right] \\
&\times \left[\frac{\pi Q a \sin(Q c)}{\tanh(\pi Q a)} - Q c \cos(Q c)\right],
\end{aligned} \tag{14}$$

with

$$c = 1.23 A^{1/3} - 0.60\,({\rm fm}), \quad a = 0.52\,({\rm fm})\,, \tag{15}$$

representing the half density radius and the diffuseness respectively. The surface thickness in this case is quantified through the relation $t = 4a\ln 3$ [34]. In Ref. [66] the first three moments entering Eq. (10) are expressed in analytical form, for the case of the Fermi symmetrized form factor, as

$$\begin{aligned}
\left\langle R_n^2 \right\rangle &= \frac{3}{5}c^2 + \frac{7}{5}(\pi a)^2 \\
\left\langle R_n^4 \right\rangle &= \frac{3}{7}c^4 + \frac{18}{7}(\pi a)^2 c^2 + \frac{31}{7}(\pi a)^4 \\
\left\langle R_n^6 \right\rangle &= \frac{1}{3}c^6 + \frac{11}{3}(\pi a)^2 c^4 + \frac{239}{15}(\pi a)^4 c^2 + \frac{127}{5}(\pi a)^6\,.
\end{aligned} \tag{16}$$

The COHERENT collaboration, has adopted the Klein-Nystrand (KN) form factor which follows from the convolution of a Yukawa potential with range $a_k = 0.7$ fm over a Woods-Saxon distribution, approximated as a hard sphere with radius $R_A$. The resulting form factor reads [65]

$$F_{\rm KN} = 3\frac{j_1(Q R_A)}{Q R_A}\left[1 + (Q a_k)^2\right]^{-1}\,, \tag{17}$$

whereas the corresponding root mean square (rms) radius becomes

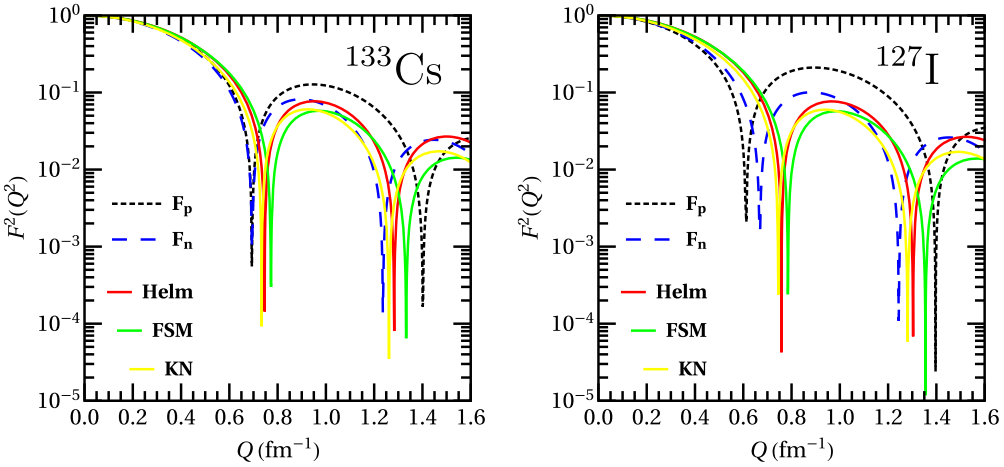


**Fig. 1.** Proton and neutron weak nuclear form factors of $^{133}$Cs (left) and $^{127}$I (right) nuclei as a function of the momentum transfer $Q\,(\mathrm{fm}^{-1})$, calculated with DSM and compared with Helm, SF and KN form factors.

$$\langle R^2\rangle_{\mathrm{KN}} = 3/5R_A^2 + 6a_k^2\,. \tag{18}$$

The form factor evaluated with DSM calculations is illustrated in Fig. 1 and is compared with the Helm, SF and KN parametrizations. As can be seen, in general, $F_p = F_n$ is not always a good approximation since minima and maxima of $F_p$ and $F_n$ occur at different values of the momentum transfer.

## 4. Results and discussion

The main results of the present work come out of a statistical analysis of the COHERENT data through the $\chi^2$ function taken from Ref. [1]

$$\chi^2(\mathcal{S}) = \min_{\xi,\zeta}\left[\sum_{i=4}^{15}\frac{\left(N^i_{\mathrm{meas}} - N^i_{\mathrm{theor}}(\mathcal{S})[1+\xi] - B^i_{0n}[1+\zeta]\right)^2}{(\sigma^i_{\mathrm{stat}})^2} + \left(\frac{\xi}{\sigma_\xi}\right)^2 + \left(\frac{\zeta}{\sigma_\zeta}\right)^2\right], \tag{19}$$

where $\xi$ and $\zeta$ are the systematic parameters to account for the uncertainties on the signal and background rates respectively, with fractional uncertainties $\sigma_\xi = 0.28$ and $\sigma_\zeta = 0.25$. The quantities $B^i_{0n}$ and $\sigma^i_{\mathrm{stat}}$ denote the $i$-th bin of the beam-on prompt neutron background events and the statistical uncertainty respectively (see Ref. [1] for details). Here, $B^i_{0n}$ is evaluated by weighting the available experimental values from the COHERENT data release [2] with the total energy delivered during the first run e.g. 7.47594 GWhr and the detector efficiency (see also Ref. [32]). In Eq. (19), $\mathcal{S}$ represents the set of parameters for which our theoretical calculation on $N_{\mathrm{theor}}(\mathcal{S})$ is evaluated. By minimizing over the nuisance parameters, we fit the COHERENT data and calculate $\Delta\chi^2(\mathcal{S}) = \chi^2(\mathcal{S}) - \chi^2_{\mathrm{min}}(\mathcal{S})$ which allows us to probe the nuclear parameters in question. Finally, in our calculations we restrict ourselves in the region $6 \leq n_{\mathrm{PE}} \leq 30$ corresponding to 12 energy bins in the range $4 \leq \mathrm{bin} \leq 15$.

The aforementioned discrepancy between the DSM and the conventional Helm, SF and KN form factors motivates us to conduct a more systematic study of the relevant nuclear physics parameters. Fig. 2 illustrates the estimated number of events within DSM, and compares the recent COHERENT data with the calculations considering the phenomenological form factors. From the left panel of this figure it can be seen that an improved agreement with the experimental data is found in the context of the employed realistic DSM calculations. Indeed, our present DSM calculations result to a better fit of the experimental data with $\chi^2_{\mathrm{min}}(\mathrm{DSM}) = 2.73$ compared to $\chi^2_{\mathrm{min}}(\mathrm{Helm}) = 3.18$, $\chi^2_{\mathrm{min}}(\mathrm{SF}) = 3.14$ and $\chi^2_{\mathrm{min}}(\mathrm{KN}) = 2.88$ evaluated in the framework of a Helm, SF and KN form factor approximations.

As demonstrated in Ref. [32] the resulted fit allows to accommodate new physics and therefore advanced nuclear physics models such as the DSM are essential for beyond the SM searches too. Despite the fact that this difference lies well within the present experimental error, we stress that future precise measurements expected during the next phases of COHERENT [46] or from the upcoming CE$\nu$NS reactor experiments [47–53] motivate the adoption of realistic nuclear structure methods especially for the accurate characterization of the nuclear target responses. For illustration purposes, the right panel of Fig. 2 depicts the difference in events between the DSM and each of the conventional form factor calculations e.g. $N_{\mathrm{Helm}} - N_{\mathrm{DSM}}$, $N_{\mathrm{SF}} - N_{\mathrm{DSM}}$ and $N_{\mathrm{KN}} - N_{\mathrm{DSM}}$ compared to the beam-on prompt neutron background events $B_{0n}$ as functions of the detected photoelectrons. For completeness, we note that the differences in events between the Helm and SF form factor calculations (not shown here) are lower than the $B_{0n}$ level.

We now focus on the current potential of the COHERENT experiment to probe important ingredients of the nuclear form factors in question. The next stages of COHERENT experiment include future upgrades with Germanium, LAr and NaI[Tl] detectors with mass up to ton-scale [2] that will not be considered in our study (we are mainly interested in the study of Cs and I isotopes). The CsI detector subsystem will continue to take data and the COHERENT Collaboration aims to reduce the statistical uncertainties [2]. We are therefore motivated to explore the attainable future sensitivities by assuming two possible upgrades, namely scenario I and II. The number of events is scaled up in terms of the factor $\mathcal{F}'$ that quantifies the exposure time, the detector mass and the SNS beam power [see Eq. (4)] while, following Ref. [34], we choose an improved statistical/systematic uncertainty. Specifically, we consider (i) a conservative future scenario I with $\mathcal{F}'/\mathcal{F} = 10$ and half systematic uncertainty compared to COHERENT first run, and (ii) an optimistic future scenario II with $\mathcal{F}'/\mathcal{F} = 100$ and a systematic uncertainty that is 25% of the first phase of COHERENT. For the statistical uncertainty in each case and more details see Table 2. Finally, in order to cover future scenarios, our calculations rely on the following $\chi^2$ function

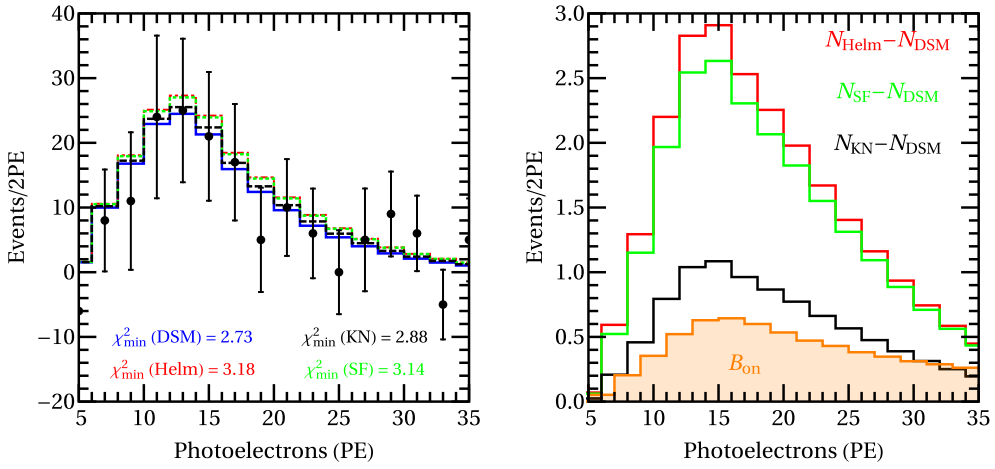


**Fig. 2.** Number of events per 2 photoelectrons at the COHERENT experiment. Left: comparison of the corresponding results calculated with DSM and conventional Helm, SF, KN form factors and the experimental data. Right: difference in events between DSM and phenomenological form factor calculations and Beam-on prompt neutron background events as a function of observed photoelectrons. For details see the text.

**Table 2**
Current and future experimental setups considered in the present study and fitted neutron rms radii.

| COHERENT | $\mathcal{F}'/\mathcal{F}$ | Stat. uncertainty | Syst. uncertainty | $\langle R_n^2\rangle^{1/2}$ (fm) |
|---|---|---|---|---|
| phase I | 1 | current [1] | current [1] | $5.64^{+0.99}_{-1.23}$ |
| scenario I | 10 | $\sigma_{\rm stat}=0.2$ | $\sigma_{\rm sys}=0.14$ | $5.23^{+0.42}_{-0.50}$ |
| scenario II | 100 | $\sigma_{\rm stat}=0.1$ | $\sigma_{\rm sys}=0.07$ | $5.23^{+0.22}_{-0.22}$ |

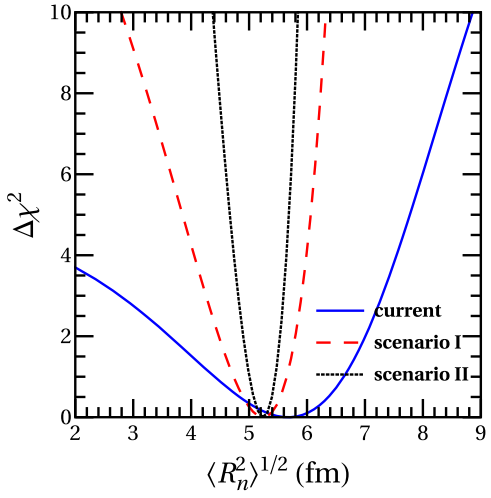


**Fig. 3.** $\Delta\chi^2$ profile of the neutron rms radius $\langle R_n^2\rangle^{1/2}$. The results are presented for different experimental setups.

$$\chi^2(\mathcal{S}) = \min_{\xi}\left[\frac{(N_{\rm DSM}-N_{\rm theor}(\mathcal{S})[1+\xi])^2}{N_{\rm DSM}(1+\sigma_{\rm stat})}+\left(\frac{\xi}{\sigma_{\rm sys}}\right)^2\right], \quad (20)$$

where in this case $N_{\rm DSM}$ denotes the number of events predicted within the context of the DSM.

In Ref. [34] it is shown that the recent CE$\nu$NS data offer a unique pathway to probe the neutron rms radius. We perform a sensitivity analysis based on the corresponding $\chi^2\left(\langle R_n^2\rangle^{1/2}\right)$ function and our present results are depicted in Fig. 3. For the current phase we find the best fit value $\langle R_n^2\rangle^{1/2}=5.64^{+0.99}_{-1.23}$ fm in good agreement with Refs. [34,60] (see Table 2), while the results do not depend significantly on the form factor used. Then, exploring the capability of a future COHERENT experiment with upgrades according to scenarios I and II we find the respective values $5.23^{+0.42}_{-0.50}$ fm in scenario I and $5.23^{+0.22}_{-0.22}$ fm in scenario II. From the latter we extract the conclusion that future COHERENT data alone (see Ref. [46] for details), will offer a better determination of $\langle R_n^2\rangle^{1/2}$ compared to the current best limit reported in Ref. [59] that was obtained through a combined analysis of the available CE$\nu$NS and APV in Cs data. It is worth mentioning that such results remain essentially unaltered regardless of the form factor used (see also Ref. [34]). We finally stress that the present work involves weak charge nuclear radii obtained from the coherent data. We note however, that a more accurate comparison with the point nucleon radii involves the "weak charge skin" [57].

We now consider the model independent expansion of the form factor given in Eq. (10). In what follows, we will consider only the neutron form factor which dominates the CE$\nu$NS process. For simplicity we take into account only the two first (even) moments and perform a combined sensitivity analysis of the current and future COHERENT data on the basis of the $\chi^2\left(\langle R_n^2\rangle,\langle R_n^4\rangle\right)$ function. In this calculation we restrict ourselves in the physical region [0,6] fm that is determined from the upper limit on $R_n(^{208}{\rm Pb})=5.75\pm0.18$ fm from the PREM experiment [57] (see also Ref. [61]). The corresponding bounds are shown in Fig. 4 at $1\sigma$, 90% and 99% C.L. The constraints are not yet competitive to current experimental results [55], while there are prospects of significant improvement in future measurements according to scenarios I and II. It can also be seen that the 4-th moment, $\langle R_n^4\rangle$, under the assumptions of the present study is not well constrained. We however emphasize that largely improved constraints are possible at multi-ton scale CE$\nu$NS detectors [44].

It is now worthwhile to explore the possibility of extracting simultaneous constraints on the parameters characterizing the Helm, SF and KN form factors, from CE$\nu$NS data. In our aim to explore the Helm form factor given in Eq. (12), we consider the parameterization $F_{\rm Helm}\left(Q^2,r_0,s\right)$ with diffraction radius $R_0=r_0A^{1/3}$ and we perform a 2-parameter fit based on the $\chi^2(r_0,s)$ function. The allowed regions in the $(r_0,s)$ plane are illustrated in the upper panel

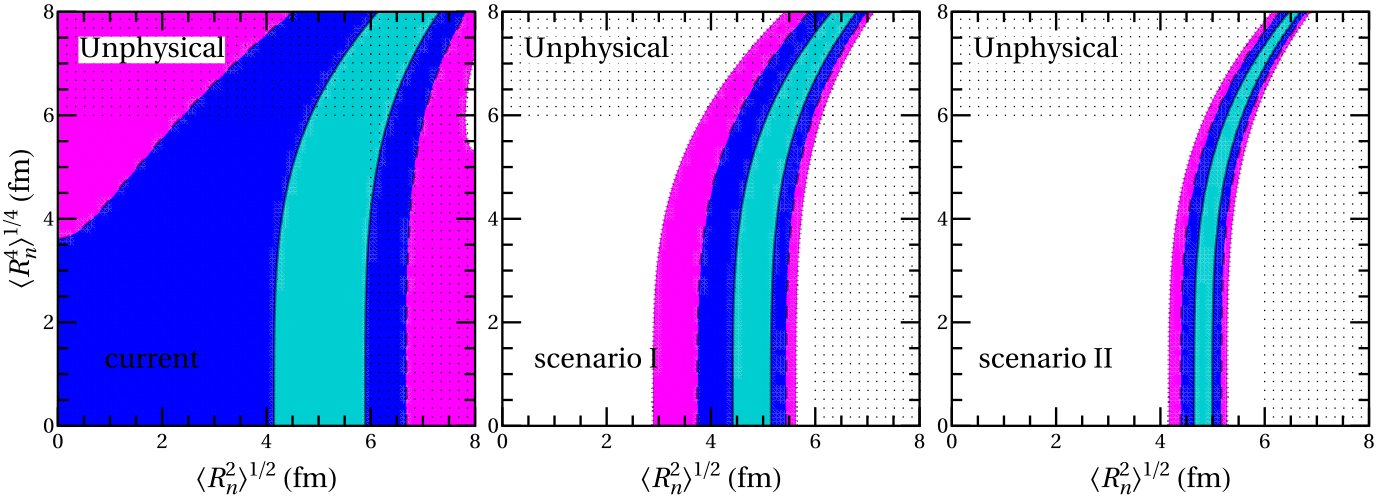


**Fig. 4.** Allowed regions in the $\langle R_n^2\rangle^{1/2}$–$\langle R_n^4\rangle^{1/4}$ parameter space from the COHERENT data for different detector specifications (see the text). The contours correspond to $1\sigma$ (turquoise), 90% C.L. (blue) and 99% C.L. (magenta).

of Fig. 5 at $1\sigma$, 90% and 99% C.L., under the assumptions of the current (phase I) and the scenarios I and II. Although it becomes evident that future measurements will drastically improve the current constraints, it can be seen that CE$\nu$NS data are not sensitive to the surface thickness, $s$. This conclusion is in agreement with a recent study of Ref. [61], while the prospect of probing $r_0$ is significant.

For the case of the SF form factor, we explore the allowed region in the $(a, c)$ parameter space. By marginalizing the relevant $\chi^2(a, c)$ function, we present the contours of the half-density radius $c$ with the surface diffuseness $a$ at $1\sigma$, 90% and 99% C.L in the middle panel of Fig. 5. The present results imply that in a future COHERENT experiment, the prospects of improvement with respect to the current constraints are rather promising and can be competitive with existing analyses [57,66] on $^{208}$Pb from PREX data [56].

In a similar way, we explore the attainable constraints on the $(R_A, a_k)$ parameters entering the KN form factor. In this case, the $1\sigma$, 90% and 99% C.L allowed regions are depicted in the lower panel of Fig. 5. Likewise, there is a large potential of improvement from future CE$\nu$NS measurements during the next phases of the COHERENT program. Finally, we perform a sensitivity fit based on the following parametrization of the effective nuclear radius [58]

$$R = r_0 A^{1/3} + r_1 \,. \tag{21}$$

Marginalizing over $r_1$, we find the best fit values

$$\begin{aligned} r_0 &= 1.28^{+0.58}_{-0.58}, \quad \text{current}\,, \\ r_0 &= 1.23^{+0.37}_{-0.27}, \quad \text{scenario I}\,, \\ r_0 &= 1.23^{+0.31}_{-0.20}, \quad \text{scenario II}\,, \end{aligned} \tag{22}$$

being consistent with Eq. (15) and Ref. [62].

## 5. Conclusions

The present work, relying on improved nuclear structure calculations employing DSM that starts with the same shell model inputs, gives a better interpretation of the current and future COHERENT data in which a large portion of the theoretical uncertainty originates from the calculation of the neutron nuclear form factors. We devoted a thorough analysis on the available CE$\nu$NS data and extracted constraints to the nuclear parameters characterizing the Helm, symmetrized Fermi and Klein-Nystrand form factor distributions. We also investigated the near- and long-term future sensitivities, within the context of two possible scenarios, and concluded that there is a large potential of improvement. We have checked that the constraints on the nuclear rms radius do not essentially depend on the form factor choice that is used to analyze the data. Moreover, we have shown that future COHERENT measurements alone will reach a better sensitivity on the neutron rms radius compared to the best current limits that were recently extracted from a combined analysis of the available data from CE$\nu$NS and APV data. Finally we have presented simultaneous constraints on the parameters characterizing the phenomenological form factors as well as for the first two moments of the neutron form factor (the sensitivity of the form factor on pairing and deformation will be studied in detail in a separate work). Reducing the latter uncertainty, possible deviations from the SM expectations may be extracted with high significance.

## Acknowledgements

DKP has been supported by the Spanish grants SEV-2014-0398 and FPA2017-85216-P (AEI/FEDER, UE), PROMETEO/2018/165 (Generalitat Valenciana) and the Spanish Red Consolider MultiDark FPA2017-90566-REDC. RS is thankful to SERB of Department of Science and Technology (Government of India) for financial support. DKP acknowledges stimulating discussions with K. Patton, C. Giunti and M. Tórtola.

## References

[1] D. Akimov, et al., Observation of coherent elastic neutrino-nucleus scattering, Science 357 (6356) (2017) 1123–1126, https://doi.org/10.1126/science.aao0990, arXiv:1708.01294.

[2] D. Akimov, et al., COHERENT Collaboration data release from the first observation of coherent elastic neutrino-nucleus scattering, arXiv:1804.09459, https://doi.org/10.5281/zenodo.1228631.

[3] H. Ejiri, J. Suhonen, K. Zuber, Neutrino–nuclear responses for astro-neutrinos, single beta decays and double beta decays, Phys. Rep. 797 (2019) 1–102, https://doi.org/10.1016/j.physrep.2018.12.001.

[4] D.K. Papoulias, T.S. Kosmas, COHERENT constraints to conventional and exotic neutrino physics, Phys. Rev. D 97 (3) (2018) 033003, https://doi.org/10.1103/PhysRevD.97.033003, arXiv:1711.09773.

[5] J. Barranco, O.G. Miranda, T.I. Rashba, Probing new physics with coherent neutrino scattering off nuclei, J. High Energy Phys. 12 (2005) 021, https://doi.org/10.1088/1126-6708/2005/12/021, arXiv:hep-ph/0508299.

[6] K. Scholberg, Prospects for measuring coherent neutrino-nucleus elastic scattering at a stopped-pion neutrino source, Phys. Rev. D 73 (2006) 033005, https://doi.org/10.1103/PhysRevD.73.033005, arXiv:hep-ex/0511042.

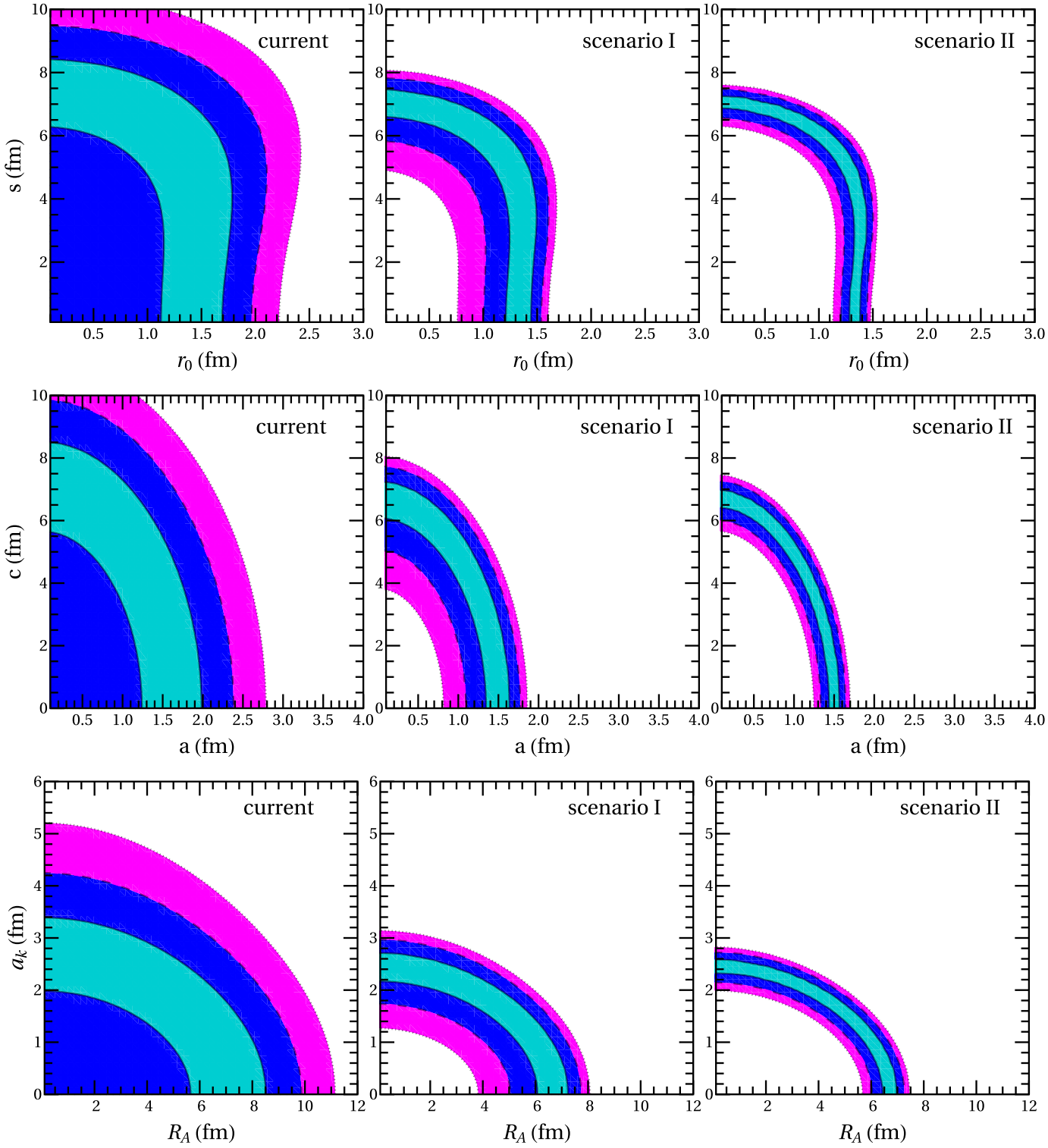


**Fig. 5.** Allowed regions in the $r_0$–$s$ (top), in the $a$–$c$ (middle) and in the $R_A$–$a_k$ (bottom) parameter space from the COHERENT data, corresponding to Helm, SF and KN form factors respectively. Different detector specifications have been considered (see the text). The results are presented at $1\sigma$, 90% C.L. and 99% C.L. (for the color coding see Fig. 4).

[7] J. Liao, D. Marfatia, COHERENT constraints on nonstandard neutrino interactions, Phys. Lett. B 775 (2017) 54–57, https://doi.org/10.1016/j.physletb.2017.10.046, arXiv:1708.04255.

[8] J.B. Dent, B. Dutta, S. Liao, J.L. Newstead, L.E. Strigari, J.W. Walker, Accelerator and reactor complementarity in coherent neutrino scattering, arXiv:1711.03521.

[9] D. Aristizabal Sierra, N. Rojas, M.H.G. Tytgat, Neutrino non-standard interactions and dark matter searches with multi-ton scale detectors, J. High Energy Phys. 03 (2018) 197, https://doi.org/10.1007/JHEP03(2018)197, arXiv:1712.09667.

[10] P.B. Denton, Y. Farzan, I.M. Shoemaker, Testing large non-standard neutrino interactions with arbitrary mediator mass after COHERENT data, J. High En-

ergy Phys. 07 (2018) 037, https://doi.org/10.1007/JHEP07(2018)037, arXiv:1804.03660.
[11] T.S. Kosmas, O.G. Miranda, D.K. Papoulias, M. Tortola, J.W.F. Valle, Probing neutrino magnetic moments at the Spallation Neutron Source facility, Phys. Rev. D 92 (1) (2015) 013011, https://doi.org/10.1103/PhysRevD.92.013011, arXiv:1505.03202.
[12] J. Billard, J. Johnston, B.J. Kavanagh, Prospects for exploring new physics in coherent elastic neutrino-nucleus scattering, arXiv:1805.01798.
[13] M. Cadeddu, C. Giunti, K.A. Kouzakov, Y.F. Li, A.I. Studenikin, Y.Y. Zhang, Neutrino charge radii from COHERENT elastic neutrino-nucleus scattering, Phys. Rev. D 98 (11) (2018) 113010, https://doi.org/10.1103/PhysRevD.98.113010, arXiv:1810.05606.
[14] T.S. Kosmas, D.K. Papoulias, M. Tortola, J.W.F. Valle, Probing light sterile neutrino signatures at reactor and Spallation Neutron Source neutrino experiments, Phys. Rev. D 96 (6) (2017) 063013, https://doi.org/10.1103/PhysRevD.96.063013, arXiv:1703.00054.
[15] B.C. Cañas, E.A. Garcés, O.G. Miranda, A. Parada, The reactor antineutrino anomaly and low energy threshold neutrino experiments, Phys. Lett. B 776 (2018) 451–456, https://doi.org/10.1016/j.physletb.2017.11.074, arXiv:1708.09518.
[16] C. Blanco, D. Hooper, P. Machado, Constraining sterile neutrino interpretations of the LSND and MiniBooNE anomalies with coherent neutrino scattering experiments, arXiv:1901.08094.
[17] J.B. Dent, B. Dutta, S. Liao, J.L. Newstead, L.E. Strigari, J.W. Walker, Probing light mediators at ultralow threshold energies with coherent elastic neutrino-nucleus scattering, Phys. Rev. D 96 (9) (2017) 095007, https://doi.org/10.1103/PhysRevD.96.095007, arXiv:1612.06350.
[18] Y. Farzan, M. Lindner, W. Rodejohann, X.-J. Xu, Probing neutrino coupling to a light scalar with coherent neutrino scattering, J. High Energy Phys. 05 (2018) 066, https://doi.org/10.1007/JHEP05(2018)066, arXiv:1802.05171.
[19] M. Abdullah, J.B. Dent, B. Dutta, G.L. Kane, S. Liao, L.E. Strigari, Coherent Elastic Neutrino Nucleus Scattering (CE$\nu$NS) as a probe of $Z'$ through kinetic and mass mixing effects, arXiv:1803.01224.
[20] V. Brdar, W. Rodejohann, X.-J. Xu, Producing a new fermion in coherent elastic neutrino-nucleus scattering: from neutrino mass to dark matter, J. High Energy Phys. 12 (2018) 024, https://doi.org/10.1007/JHEP12(2018)024, arXiv:1810.03626.
[21] O.G. Miranda, D.K. Papoulias, M. Tórtola, J.W.F. Valle, Probing neutrino transition magnetic moments with coherent elastic neutrino-nucleus scattering, arXiv:1905.03750.
[22] D. Aristizabal Sierra, V. De Romeri, N. Rojas, CP violating effects in coherent elastic neutrino-nucleus scattering processes, arXiv:1906.01156.
[23] S.-F. Ge, I.M. Shoemaker, Constraining photon portal dark matter with texono and coherent data, arXiv:1710.10889.
[24] P. Coloma, M.C. Gonzalez-Garcia, M. Maltoni, T. Schwetz, COHERENT enlightenment of the neutrino dark side, Phys. Rev. D 96 (11) (2017) 115007, https://doi.org/10.1103/PhysRevD.96.115007, arXiv:1708.02899.
[25] M.C. Gonzalez-Garcia, M. Maltoni, Y.F. Perez-Gonzalez, R. Zukanovich Funchal, Neutrino discovery limit of dark matter direct detection experiments in the presence of non-standard interactions, J. High Energy Phys. 07 (2018) 019, https://doi.org/10.1007/JHEP07(2018)019, arXiv:1803.03650.
[26] K.C.Y. Ng, J.F. Beacom, A.H.G. Peter, C. Rott, Solar atmospheric neutrinos: a new neutrino floor for dark matter searches, Phys. Rev. D 96 (10) (2017) 103006, https://doi.org/10.1103/PhysRevD.96.103006, arXiv:1703.10280.
[27] D.K. Papoulias, R. Sahu, T.S. Kosmas, V.K.B. Kota, B. Nayak, Novel neutrino-floor and dark matter searches with deformed shell model calculations, Adv. High Energy Phys. 2018 (2018) 6031362, https://doi.org/10.1155/2018/6031362, arXiv:1804.11319.
[28] C. Bœhm, D.G. Cerdeño, P.A.N. Machado, A.O.-D. Campo, E. Reid, How high is the neutrino floor? J. Cosmol. Astropart. Phys. 1901 (2019) 043, https://doi.org/10.1088/1475-7516/2019/01/043, arXiv:1809.06385.
[29] B. Dutta, L.E. Strigari, Neutrino physics with dark matter detectors, arXiv:1901.08876.
[30] V.A. Bednyakov, D.V. Naumov, Coherency and incoherency in neutrino-nucleus elastic and inelastic scattering, Phys. Rev. D 98 (5) (2018) 053004, https://doi.org/10.1103/PhysRevD.98.053004, arXiv:1806.08768.
[31] M. Lindner, W. Rodejohann, X.-J. Xu, Coherent neutrino-nucleus scattering and new neutrino interactions, J. High Energy Phys. 03 (2017) 097, https://doi.org/10.1007/JHEP03(2017)097, arXiv:1612.04150.
[32] D. Aristizabal Sierra, V. De Romeri, N. Rojas, COHERENT analysis of neutrino generalized interactions, Phys. Rev. D 98 (2018) 075018, https://doi.org/10.1103/PhysRevD.98.075018, arXiv:1806.07424.
[33] O.G. Miranda, G.S. Garcia, O. Sanders, Testing new physics with future COHERENT experiments, arXiv:1902.09036.
[34] M. Cadeddu, C. Giunti, Y.F. Li, Y.Y. Zhang, Average CsI neutron density distribution from COHERENT data, Phys. Rev. Lett. 120 (7) (2018) 072501, https://doi.org/10.1103/PhysRevLett.120.072501, arXiv:1710.02730.
[35] V.K.B. Kota, R. Sahu, Structure of Medium Mass Nuclei: Deformed Shell Model and Spin-Isospin Interacting Boson Model, CRC Press, 2016, URL https://www.amazon.com/Structure-Medium-Mass-Nuclei-Spin-Isospin-ebook/dp/B01MTZWTUT?SubscriptionId=0JYN1NVW651KCA56C102&tag=techkie-20&linkCode=xm2&camp=2025&creative=165953&creativeASIN=B01MTZWTUT.
[36] R. Sahu, P.C. Srivastava, V.K.B. Kota, Deformed shell model results for neutrinoless positron double beta decay of nuclei in the A = 60–90 region, J. Phys. G 40 (2013) 095107, https://doi.org/10.1088/0954-3899/40/9/095107.
[37] R. Sahu, V.K.B. Kota, Deformed shell model results for neutrinoless double beta decay of nuclei in A = 60 - 90 region, Int. J. Mod. Phys. E 24 (03) (2015) 1550022, https://doi.org/10.1142/S0218301315500226, arXiv:1409.4929.
[38] T.S. Kosmas, A. Faessler, R. Sahu, Transition matrix elements for mu e conversion in ge-72 using the deformed Hartree-Fock method, Phys. Rev. C 68 (2003) 054315, https://doi.org/10.1103/PhysRevC.68.054315.
[39] R. Sahu, V.K.B. Kota, Deformed shell model study of event rates for WIMP-$^{73}$Ge scattering, Mod. Phys. Lett. A 32 (38) (2017) 1750210, https://doi.org/10.1142/S0217732317502108, arXiv:1706.08112.
[40] D.K. Papoulias, T.S. Kosmas, Standard and nonstandard neutrino-nucleus reactions cross sections and event rates to neutrino detection experiments, Adv. High Energy Phys. 2015 (2015) 763648, https://doi.org/10.1155/2015/763648, arXiv:1502.02928.
[41] P. Pirinen, J. Suhonen, E. Ydrefors, Neutral-current neutrino-nucleus scattering off Xe isotopes, Adv. High Energy Phys. 2018 (2018) 9163586, https://doi.org/10.1155/2018/9163586, arXiv:1804.08995.
[42] T.S. Kosmas, O.G. Miranda, D.K. Papoulias, M. Tortola, J.W.F. Valle, Sensitivities to neutrino electromagnetic properties at the TEXONO experiment, Phys. Lett. B 750 (2015) 459–465, https://doi.org/10.1016/j.physletb.2015.09.054, arXiv:1506.08377.
[43] B.C. Cañas, E.A. Garcés, O.G. Miranda, A. Parada, Future perspectives for a weak mixing angle measurement in coherent elastic neutrino nucleus scattering experiments, Phys. Lett. B 784 (2018) 159–162, https://doi.org/10.1016/j.physletb.2018.07.049, arXiv:1806.01310.
[44] K. Patton, J. Engel, G.C. McLaughlin, N. Schunck, Neutrino-nucleus coherent scattering as a probe of neutron density distributions, Phys. Rev. C 86 (2012) 024612, https://doi.org/10.1103/PhysRevC.86.024612, arXiv:1207.0693.
[45] E. Ciuffoli, J. Evslin, Q. Fu, J. Tang, Extracting nuclear form factors with coherent neutrino scattering, Phys. Rev. D 97 (11) (2018) 113003, https://doi.org/10.1103/PhysRevD.97.113003, arXiv:1801.02166.
[46] D. Akimov, et al., COHERENT 2018 at the Spallation Neutron Source, arXiv:1803.09183.
[47] H.T. Wong, Neutrino-nucleus coherent scattering and dark matter searches with sub-keV germanium detector, Nucl. Phys. A 844 (2010) 229C–233C, https://doi.org/10.1016/j.nuclphysa.2010.05.040.
[48] A. Aguilar-Arevalo, et al., Results of the engineering run of the Coherent Neutrino Nucleus Interaction Experiment (CONNIE), J. Instrum. 11 (07) (2016) P07024, https://doi.org/10.1088/1748-0221/11/07/P07024, arXiv:1604.01343.
[49] G. Agnolet, et al., Background studies for the MINER coherent neutrino scattering reactor experiment, Nucl. Instrum. Methods A 853 (2017) 53–60, https://doi.org/10.1016/j.nima.2017.02.024, arXiv:1609.02066.
[50] V. Belov, et al., The GeN experiment at the Kalinin Nuclear Power Plant, J. Instrum. 10 (12) (2015) P12011, https://doi.org/10.1088/1748-0221/10/12/P12011.
[51] Private communication with CONUS collaboration.
[52] J. Billard, et al., Coherent neutrino scattering with low temperature bolometers at Chooz reactor complex, J. Phys. G 44 (10) (2017) 105101, https://doi.org/10.1088/1361-6471/aa83d0, arXiv:1612.09035.
[53] R. Strauss, et al., The $\nu$-cleus experiment: a gram-scale fiducial-volume cryogenic detector for the first detection of coherent neutrino-nucleus scattering, Eur. Phys. J. C 77 (2017) 506, https://doi.org/10.1140/epjc/s10052-017-5068-2, arXiv:1704.04320.
[54] G. Fricke, C. Bernhardt, K. Heilig, L.A. Schaller, L. Schellenberg, E.B. Shera, C.W. de Jager, Nuclear ground state charge radii from electromagnetic interactions, At. Data Nucl. Data Tables 60 (1995) 177–285, https://doi.org/10.1006/adnd.1995.1007.
[55] I. Angeli, K.P. Marinova, Table of experimental nuclear ground state charge radii: an update, At. Data Nucl. Data Tables 99 (1) (2013) 69–95, https://doi.org/10.1016/j.adt.2011.12.006.
[56] S. Abrahamyan, et al., Measurement of the neutron radius of 208Pb through parity-violation in electron scattering, Phys. Rev. Lett. 108 (2012) 112502, https://doi.org/10.1103/PhysRevLett.108.112502, arXiv:1201.2568.
[57] C.J. Horowitz, et al., Weak charge form factor and radius of 208Pb through parity violation in electron scattering, Phys. Rev. C 85 (2012) 032501, https://doi.org/10.1103/PhysRevC.85.032501, arXiv:1202.1468.
[58] S.E.A. Orrigo, L. Alvarez-Ruso, C. Peña-Garay, A new approach to nuclear form factors for direct dark matter searches, Nucl. Part. Phys. Proc. 273–275 (2016) 414–418, https://doi.org/10.1016/j.nuclphysbps.2015.09.060.
[59] M. Cadeddu, F. Dordei, Reinterpreting the weak mixing angle from atomic parity violation in view of the Cs neutron rms radius measurement from COHERENT, Phys. Rev. D 99 (3) (2019) 033010, https://doi.org/10.1103/PhysRevD.99.033010, arXiv:1808.10202.
[60] X.-R. Huang, L.-W. Chen, Neutron skin in CsI and low-energy effective weak mixing angle from COHERENT data, arXiv:1902.07625.

[61] D. Aristizabal Sierra, J. Liao, D. Marfatia, Impact of form factor uncertainties on interpretations of coherent elastic neutrino-nucleus scattering data, arXiv:1902.07398.
[62] J.D. Lewin, P.F. Smith, Review of mathematics, numerical factors, and corrections for dark matter experiments based on elastic nuclear recoil, Astropart. Phys. 6 (1996) 87–112, https://doi.org/10.1016/S0927-6505(96)00047-3.
[63] R.H. Helm, Inelastic and elastic scattering of 187-Mev electrons from selected even-even nuclei, Phys. Rev. 104 (1956) 1466–1475, https://doi.org/10.1103/PhysRev.104.1466.
[64] D.W.L. Sprung, J. Martorell, The symmetrized Fermi function and its transforms, J. Phys. A, Math. Gen. 30 (18) (1997) 6525–6534, https://doi.org/10.1088/0305-4470/30/18/026.
[65] S. Klein, J. Nystrand, Exclusive vector meson production in relativistic heavy ion collisions, Phys. Rev. C 60 (1999) 014903, https://doi.org/10.1103/PhysRevC.60.014903, arXiv:hep-ph/9902259.
[66] J. Piekarewicz, A.R. Linero, P. Giuliani, E. Chicken, Power of two: assessing the impact of a second measurement of the weak-charge form factor of $^{208}$Pb, Phys. Rev. C 94 (3) (2016) 034316, https://doi.org/10.1103/PhysRevC.94.034316, arXiv:1604.07799.
[67] http://www.nndc.bnl.gov/ensdf.
[68] J. Beringer, et al., Rev. Part. Phys. (RPP), Phys. Rev. D 86 (2012) 010001, https://doi.org/10.1103/PhysRevD.86.010001.
[69] J. Suhonen, Impact of the quenching of $g_A$ on the sensitivity of $0\nu\beta\beta$ experiments, Phys. Rev. C 96 (5) (2017) 055501, https://doi.org/10.1103/PhysRevC.96.055501, arXiv:1708.09604.
[70] J.I. Collar, N.E. Fields, M. Hai, T.W. Hossbach, J.L. Orrell, C.T. Overman, G. Perumpilly, B. Scholz, Coherent neutrino-nucleus scattering detection with a CsI[Na] scintillator at the SNS spallation source, Nucl. Instrum. Methods A 773 (2015) 56–65, https://doi.org/10.1016/j.nima.2014.11.037, arXiv:1407.7524.
[71] M. Kortelainen, J. Suhonen, J. Toivanen, T.S. Kosmas, Event rates for CDM detectors from large-scale shell-model calculations, Phys. Lett. B 632 (2006) 226–232, https://doi.org/10.1016/j.physletb.2005.10.057.
[72] P. Toivanen, M. Kortelainen, J. Suhonen, J. Toivanen, Large-scale shell-model calculations of elastic and inelastic scattering rates of lightest supersymmetric particles (LSP) on I-127, Xe-129, Xe-131, and Cs-133 nuclei, Phys. Rev. C 79 (2009) 044302, https://doi.org/10.1103/PhysRevC.79.044302.
[73] D. Papoulias, T. Kosmas, Nuclear aspects of neutral current non-standard $\nu$-nucleus reactions and the role of the exotic $\mu^- \to e^-$ transitions experimental limits, Phys. Lett. B 728 (2014) 482–488, https://doi.org/10.1016/j.physletb.2013.12.028, arXiv:1312.2460.
[74] L. Coraggio, L. De Angelis, T. Fukui, A. Gargano, N. Itaco, Calculation of Gamow-Teller and two-neutrino double–decay properties for $^{130}$Te and $^{136}$Xe with a realistic nucleon-nucleon potential, Phys. Rev. C 95 (6) (2017) 064324, https://doi.org/10.1103/PhysRevC.95.064324, arXiv:1703.05087.
[75] C.G. Payne, S. Bacca, G. Hagen, W. Jiang, T. Papenbrock, Coherent elastic neutrino-nucleus scattering on $^{40}$Ar from first principles, arXiv:1908.09739 [nucl-th].
[76] Junjie Yang, Jesse A. Hernandez, J. Piekarewicz, Electroweak probes of ground state densities, Phys. Rev. C 100 (2019) 054301, https://doi.org/10.1103/PhysRevC.100.054301, arXiv:1908.10939 [nucl-th].
[77] T. Smponias, O.T. Kosmas, High energy neutrino emission from astrophysical jets in the galaxy, Adv. High Energy Phys. 2015 (2015) 921757, https://doi.org/10.1155/2015/921757.
[78] F.J. Fattoyev, J. Piekarewicz, C.J. Horowitz, Neutron skins and neutron stars in the multimessenger era, Phys. Rev. Lett. 120 (2018) 172702, https://doi.org/10.1103/PhysRevLett.120.172702, arXiv:1711.06615 [nucl-th].